



# How do Cl concentrations matter for simulating CH<sub>4</sub>, δ<sup>13</sup>C(CH<sub>4</sub>) and estimating CH<sub>4</sub> budget through atmospheric inversions ?

Joël Thanwerdas<sup>1,\*</sup>, Marielle Saunois<sup>1</sup>, Isabelle Pison<sup>1</sup>, Didier Hauglustaine<sup>1</sup>, Antoine Berchet<sup>1</sup>, Bianca Baier<sup>2,3</sup>, Colm Sweeney<sup>3</sup>, and Philippe Bousquet<sup>1</sup>

<sup>1</sup>Laboratoire des Sciences du Climat et de l'Environnement, LSCE-IPSL (CEA-CNRS-UVSQ), Université Paris-Saclay 91191 Gif-sur-Yvette, France.

<sup>2</sup>Cooperative Institute for Research in Environmental Sciences (CIRES), University of Colorado-Boulder, Boulder, CO, USA 80305.

<sup>3</sup>NOAA Earth System Research Laboratory Global Monitoring Division, Boulder, CO, USA 80305.

**Correspondence:** J. Thanwerdas (joel.thanwerdas@lscce.ipsl.fr)

**Abstract.** Atmospheric methane (CH<sub>4</sub>) concentrations have been rising since 2007, resulting from an imbalance between CH<sub>4</sub> sources and sinks. The CH<sub>4</sub> budget is generally estimated through top-down approaches using CH<sub>4</sub> observations as constraints. The atmospheric isotopic CH<sub>4</sub> signal, δ<sup>13</sup>C(CH<sub>4</sub>), can also provide additional constraints and helps to discriminate between emission categories. The oxidation by chlorine (Cl) likely contributes less than 5 % to the total oxidation of atmospheric CH<sub>4</sub>. However, the Cl sink is highly fractionating, and thus strongly influences δ<sup>13</sup>C(CH<sub>4</sub>). As inversion studies do not prescribe the same Cl fields to constrain CH<sub>4</sub> budget, it can lead to discrepancies between estimates. To quantify the influence of the Cl concentrations on CH<sub>4</sub>, δ<sup>13</sup>C(CH<sub>4</sub>) and CH<sub>4</sub> budget estimates, we perform multiple sensitivity simulations using three Cl fields with concentrations that are realistic with regard to recent literature and one Cl field with concentrations that are very likely to be overestimated. We also test removing the tropospheric and the entire Cl sink in other sensitivity simulations. We find that the realistic Cl fields tested here are responsible for between 0.3 % and 1.8 % of the total chemical CH<sub>4</sub> sink in the troposphere and between 1.0 % and 1.2 % in the stratosphere. Prescribing these different Cl amounts in surface-based inversions can lead to differences in global CH<sub>4</sub> source adjustments of up to 12.3 TgCH<sub>4</sub>.yr<sup>-1</sup>. We also find that the globally-averaged isotopic signature of the CH<sub>4</sub> sources inferred by a surface-based inversion assimilating δ<sup>13</sup>C(CH<sub>4</sub>) observations would decrease by 0.53 ‰ for each additional percent of contribution from the tropospheric Cl sink to the total sink. Finally, our study shows that CH<sub>4</sub> seasonal cycle amplitude is modified by less than 1-2 % but δ<sup>13</sup>C(CH<sub>4</sub>) seasonal cycle amplitude can be modified by up to 10-20 %, depending on the latitude.

## 1 Introduction

Methane (CH<sub>4</sub>) is a very important species for both atmospheric chemistry and climate. Its atmospheric mole fractions have reached an average of 1879 ppb at the surface in 2020 (Dlugokencky, 2021), almost three times higher than pre-industrial mole fractions (Etheridge et al., 1998). After a plateau between 1999 and 2006, CH<sub>4</sub> mole fractions resumed their increase in 2007 without showing any sign of stabilization since then. The increase has even reached an unprecedented value of +15.9 ppb



for the year 2020. The accumulation of CH<sub>4</sub> (~ 8 ppb.yr<sup>-1</sup> on average since 2007) in the atmosphere is the result of a slight imbalance between sources that release CH<sub>4</sub> into the atmosphere and sinks that remove it. Sinks are mostly due to oxidation reactions in the atmosphere. Three radicals react with CH<sub>4</sub> in the atmosphere: hydroxyl (OH), atomic oxygen (O<sup>1</sup>D), and chlorine (Cl). These chemical reactions account for about 93 % of the total CH<sub>4</sub> sink, with the remainder being removed by methanotrophic bacteria in the soil (Saunio et al., 2020). On the other hand, CH<sub>4</sub> sources are varied and result from radically different processes (biogenic, thermogenic and pyrogenic).

Top-down atmospheric inversions are known to be efficient approaches to estimate CH<sub>4</sub> sources at different scales and have become increasingly relevant over the years as observational networks have developed (Houweling et al., 2017, and references therein). However, inversions that assimilate only total CH<sub>4</sub> observations can only rely on variations in seasonal cycles to differentiate co-located emissions. To better separate these sources, assimilating observations of the <sup>13</sup>C:<sup>12</sup>C atmospheric isotope signal of CH<sub>4</sub>, denoted δ<sup>13</sup>C(CH<sub>4</sub>), can be relevant. This value is based on the ratio between the isotopologue <sup>12</sup>CH<sub>4</sub>, which represents about 99 % of the CH<sub>4</sub> in the atmosphere (Stolper et al., 2014) and its counterpart <sup>13</sup>CH<sub>4</sub>. δ<sup>13</sup>C(CH<sub>4</sub>) is commonly defined using a deviation of the sample mole isotopic ratio relative to a specific standard ratio :

$$\delta^{13}\text{C}(\text{CH}_4) = \frac{R}{R_{\text{std}}} - 1 = \frac{[^{13}\text{CH}_4]/[^{12}\text{CH}_4]}{R_{\text{std}}} - 1 \quad (1)$$

[<sup>12</sup>CH<sub>4</sub>] and [<sup>13</sup>CH<sub>4</sub>] denote the <sup>12</sup>CH<sub>4</sub> and <sup>13</sup>CH<sub>4</sub> mole fractions, respectively. R<sub>std</sub> = 0.0112372 is here the standard ratio of Pee Dee Belemnite (PDB) (Craig, 1957). CH<sub>4</sub> sources exhibit specific isotopic signatures that are mainly controlled by the process involved. Broadly summarized, most biogenic sources have an isotopic signature between -65 and -55 ‰, thermogenic sources between -50 and -30 ‰ and pyrogenic sources between -25 ‰ and -15 ‰ (Sherwood et al., 2017), although the distributions are very large and overlaps exist between the extreme values. The post-2007 CH<sub>4</sub> increase is notably associated with a decrease in the atmospheric isotopic signal δ<sup>13</sup>C(CH<sub>4</sub>) (Nisbet et al., 2019) and these isotopic variations could help to better explain this renewed growth and the contribution from the different CH<sub>4</sub> sources.

The sinks are also fractionating, as they remove <sup>12</sup>CH<sub>4</sub> faster than <sup>13</sup>CH<sub>4</sub>. This effect, called the Kinetic Isotope Effect (KIE), is quantified using the ratio of the reaction rate constants X + <sup>12</sup>CH<sub>4</sub> and X + <sup>13</sup>CH<sub>4</sub>, with X the species of interest (X = OH, O<sup>1</sup>D) or Cl). KIE<sub>X</sub> = k<sub>12</sub><sup>X</sup>/k<sub>13</sub><sup>X</sup> with k<sub>12</sub><sup>X</sup> and k<sub>13</sub><sup>X</sup> being the oxidation reaction rate constants. As a result, δ<sup>13</sup>C(CH<sub>4</sub>) depends on both sources and sinks, as total CH<sub>4</sub>, but also on the isotopic fractionation and the sources isotopic signatures.

Among all CH<sub>4</sub> sinks, the Cl sink accounts for a small part of the total CH<sub>4</sub> oxidation. Following the discovery of the dramatic impact of Cl on ozone in the stratosphere, many studies have first focused on the impact of stratospheric Cl on CH<sub>4</sub> and δ<sup>13</sup>C(CH<sub>4</sub>) using box or 2-D models (e.g., Röckmann et al., 2004; McCarthy et al., 2003; Wang et al., 2002; McCarthy et al., 2001; Saueressig et al., 2001; Gupta et al., 1996; Müller et al., 1996). McCarthy et al. (2003) estimated that Cl was responsible for 20-35 % of CH<sub>4</sub> removal in the stratosphere. Saunio et al. (2020) suggested a range of values for the total stratospheric sink between 12 and 37 TgCH<sub>4</sub>.yr<sup>-1</sup>, leading to a plausible stratospheric Cl sink of 2-13 TgCH<sub>4</sub>.yr<sup>-1</sup>, or about only 0.4-2.4 % of the total CH<sub>4</sub> oxidation in the atmosphere. Although this contribution is very small, the Cl sink is particularly important because of its large fractionation effect (KIE = 1.066 for the Cl sink against 1.0039 for the OH sink, see Sect. 2.1). The aforementioned studies showed that stratospheric Cl has a strong impact on δ<sup>13</sup>C(CH<sub>4</sub>) not only in the stratosphere but also



at the surface. In particular, Wang et al. (2002) estimated that stratospheric Cl was responsible for a  $\delta^{13}\text{C}(\text{CH}_4)$  enhancement of 0.23 ‰ at the surface between 1970 and 1992 due to stratosphere-troposphere exchanges (STE).

In the troposphere, the Cl sink likely accounts for less than 5 % of  $\text{CH}_4$  oxidation (Wang et al., 2019, 2021; Hossaini et al., 2016; Sherwen et al., 2016; Gromov et al., 2018; Allan et al., 2007). Several studies have estimated Cl concentrations in the troposphere and in the Marine Boundary Layer (MBL) and discussed the Cl sink. Allan et al. (2007) estimated the Cl sink in the troposphere to be 25  $\text{TgCH}_4\cdot\text{yr}^{-1}$ , representing about 5 % of the total  $\text{CH}_4$  chemical sink. More recently, Hossaini et al. (2016), Sherwen et al. (2016), Wang et al. (2019) and Wang et al. (2021) have made important developments in tropospheric chemistry modeling and obtained oxidation contributions of 2.6 %, 2 %, 1 % and 0.8 % respectively with mean tropospheric Cl concentrations between 620 and 1300  $\text{molec}\cdot\text{cm}^{-3}$ . However, Gromov et al. (2018) concluded that variations in Cl concentrations above 900  $\text{molec}\cdot\text{cm}^{-3}$  in the extratropical part of the Southern Hemisphere are very unlikely ; thus suggesting that the high estimates from Allan et al. (2007) and Hossaini et al. (2016) are likely overestimated. These variations in oxidation contributions may appear small but Strode et al. (2020) recently showed a high sensitivity of the tropospheric  $\delta^{13}\text{C}(\text{CH}_4)$  distribution to variation in Cl fields by testing, among others, those of Allan et al. (2007), Sherwen et al. (2016) and Hossaini et al. (2016), indicating that each percent increase in how much  $\text{CH}_4$  is oxidized by Cl leads to a 0.5 ‰ increase in  $\delta^{13}\text{C}(\text{CH}_4)$ , therefore larger than the global downward shift observed since 2007 (Nisbet et al., 2019).

Forward and inverse 3-D modeling studies focusing on  $\text{CH}_4$  and  $\delta^{13}\text{C}(\text{CH}_4)$  consider the Cl sink at different level of details. Most studies consider only the Cl sink in the stratosphere (e.g., Fujita et al., 2020; Rigby et al., 2012; Monteil et al., 2011; Fletcher et al., 2004), and a very few account for tropospheric Cl only (e.g., Thompson et al., 2018). In single-box models, sinks are combined and an overall fractionation coefficient is used (e.g., Schaefer et al., 2016; Schwietzke et al., 2016). In recent studies, Cl is often prescribed in both the troposphere and stratosphere (e.g., McNorton et al., 2018; Rice et al., 2016; Warwick et al., 2016; Neef et al., 2010), although most studies use the Cl configuration suggested by Allan et al. (2007), which is likely to be overestimated as mentioned above.

In the atmospheric inversions performed with the LMDz-SACS chemistry-transport model (Locatelli et al., 2015; Pison et al., 2009), Cl sink was omitted so far, even in the stratosphere (Saunois et al., 2020; Locatelli et al., 2015; Pison et al., 2009; Bousquet et al., 2006). For these studies assimilating only total  $\text{CH}_4$  observations, the impact of the Cl sink on the estimated  $\text{CH}_4$  emissions was considered negligible. However, the number and quality of isotopic observations have considerably increased since the 2000s, and developments of the CIF-LMDz-SACS inversion system to use the isotopic constraint have been made (Thanwerdas et al., 2021). Joint assimilation ( $\text{CH}_4$  and  $\delta^{13}\text{C}(\text{CH}_4)$ ) is proving to be relevant and necessary in order to reconcile the estimated  $\text{CH}_4$  budgets with the atmospheric isotope signal. Considering the large impact of the Cl sink on  $\delta^{13}\text{C}(\text{CH}_4)$ , it is necessary to include and evaluate the Cl sink and its impact on the  $\text{CH}_4$  modeling process.

Here, we detail the influence of tropospheric and stratospheric Cl on the modeling of  $\text{CH}_4$  and  $\delta^{13}\text{C}(\text{CH}_4)$  in LMDz-SACS by using several Cl fields. Ultimate goal being to use the isotopic signal observations to perform multi-constraint inversions with the LMDz-SACS model, results are analyzed throughout the study under the prism of atmospheric inversion. In the first part, we present the characteristics of the available Cl fields, model inputs and observations used for evaluation. Then, we analyze the influence of the different Cl fields on  $\text{CH}_4$  and  $\delta^{13}\text{C}(\text{CH}_4)$  at the surface and on the  $\text{CH}_4$  vertical profile.



## 2 Methods

### 2.1 The chemistry-transport model

The general circulation model (GCM) LMDz is the atmospheric component of the coupled model of the Institut Pierre-Simon Laplace (IPSL-CM) developed at the Laboratoire de Météorologie Dynamique (LMD) (Hourdin et al., 2006). The version of LMDz used here is an "offline" version dedicated to the inversion framework created by Chevallier et al. (2005): the pre-calculated meteorological fields provided by the online version of LMDz are given as input to the model, which considerably reduces the computation time. The model is built at a horizontal resolution of  $3.8^\circ \times 1.9^\circ$  (96 grid cells in longitude and latitude) with 39 hybrid sigma pressure levels reaching an altitude of about 75 km. About 20 levels are dedicated to the stratosphere and the mesosphere. The time step of the model is 30 min and the output values have a resolution of 3 hours. Horizontal winds have been nudged towards the ECMWF meteorological analyses (ERA-Interim) in the online version of the model. Vertical diffusion is parameterised by a local approach of Louis (1979), and deep convection processes are parameterised by the scheme of Tiedtke (1989). The offline model LMDz, coupled with the Simplified Atmospheric Chemistry System (SACS) module (Pison et al., 2009), was previously used to simulate atmospheric mole fractions of trace gases such as CH<sub>4</sub>, carbon monoxide (CO), methyl chloroform (MCF), formaldehyde (CH<sub>2</sub>O) or hydrogen (H<sub>2</sub>). This system has been recently converted into a chemistry parsing system (Thanwerdas et al., 2021). It follows the principle of the chemical parsing system of the regional model CHIMERE (Mailler et al., 2017; Menut et al., 2013) and allows the user to prescribe the set of chemical reactions to consider. Consequently, it generalizes the SACS module to any set of possible reactions. The concentration fields of the different species are either prescribed or simulated. Prescribed species (here OH, O(<sup>1</sup>D) and Cl) are not transported in LMDz, and their mole fractions are not updated by chemical production or destruction. These species are only used to calculate reaction rates and update the mole fractions of transported species at each iteration of the model. In this study, the <sup>12</sup>CH<sub>4</sub> and <sup>13</sup>CH<sub>4</sub> isotopologues are simulated as separate tracers and CH<sub>4</sub> mole fractions are defined as a sum of mole fractions of the two isotopologues. Oxidation by Cl + CH<sub>4</sub> was added to complete the chemical removal of CH<sub>4</sub>, which only considered OH + CH<sub>4</sub> and O(<sup>1</sup>D) + CH<sub>4</sub> reactions in the original SACS chemical scheme.

Reactions between <sup>12</sup>CH<sub>4</sub> and OH, O(<sup>1</sup>D) and Cl are represented by the chemical equations below, and similar equations apply to <sup>13</sup>CH<sub>4</sub> :



Three-dimensional and time-dependent oxidant concentration fields (OH, O(<sup>1</sup>D) and Cl) were simulated by the GCM LMDz coupled to the INteraction with Chemistry and Aerosols (INCA) model (Hauglustaine et al., 2021; Folberth et al., 2006; Hauglustaine et al., 2004). Seventeen ozone-depleting substances consisted of CFCs (CFC-12, CFC-11, CFC-113), three HCFCs (HCFC-22, HCFC-141b, HCFC-142b), two halons (Halon-1211, Halon-1301), methyl chloroform (CH<sub>3</sub>CCl<sub>3</sub>), carbon



125 tetrachloride (CCl<sub>4</sub>), methylchloride (CH<sub>3</sub>Cl), methylene chloride (CH<sub>2</sub>Cl<sub>2</sub>), chloroform (CHCl<sub>3</sub>), methyl bromide (CH<sub>3</sub>Br) and HFC-134a, and their associated photochemical reactions, were included in the INCA chemical scheme to produce Cl radicals (Terrenoire et al., 2020). In the LMDz-INCA simulations, surface concentrations of these long-lived Cl source species were prescribed based on historical data sets prepared by Meinshausen et al. (2017). The model was run for the 1850-2018 period (Hauglustaine et al., 2021).

**Table 1.** Reaction rate constants and KIEs of CH<sub>4</sub> chemical sinks. The reaction rate constants are taken from Burkholder et al. (2015).

Oxidant	KIE	Reference	Reaction rate constant (cm <sup>3</sup> molec <sup>-1</sup> s <sup>-1</sup> )
OH	1.0039	Saueressig et al. (2001)	$2.45 \times 10^{-12} \cdot \exp(-1775/T)$
Cl	$1.043 \cdot \exp(6.455/T)$	Saueressig et al. (1995)	$7.1 \times 10^{-12} \cdot \exp(-1280/T)$
O( <sup>1</sup> D) - R3	1.013	Saueressig et al. (2001)	$1.125 \times 10^{-10}$
O( <sup>1</sup> D) - R4	1.013	Saueressig et al. (2001)	$3.75 \times 10^{-11}$

130 All reaction rate constants and associated values are given in Table 1. The reaction rate constants with <sup>13</sup>CH<sub>4</sub> are modified based on the definition of the fractionation coefficient (KIE). Few studies have evaluated the KIEs associated with CH<sub>4</sub> chemical sinks (particularly for O(<sup>1</sup>D) and Cl) over a wide range of temperatures and thus large uncertainties remain. For CH<sub>4</sub> + OH, we adopted the value of Saueressig et al. (2001) as they indicate that this data is of considerably higher experimental precision and reproducibility than previous studies, in particular Cantrell et al. (1990), which suggested a value of 1.0054.

## 2.2 Description of Cl fields

135 Four fields of Cl are used in this study. The first field was simulated by the LMDz-INCA model, as mentioned above. More details on the modeling of this field are available in the supplement. This field will be referred to as the Cl-INCA field. At this stage, simulations performed with the LMDz-INCA model do not fully represent the chemical interactions between Cl and other species in the troposphere. Developments are currently being made to improve these interactions. The mean tropospheric Cl concentration (330 molec.cm<sup>-3</sup>) in the Cl-INCA field is therefore about half lower than the mean tropospheric value (630 molec.cm<sup>-3</sup>) of Wang et al. (2021) or other studies, but in agreement with the upper limits inferred by Gromov et al. (2018).

145 Two fields were simulated using the versions of the GEOS-Chem model (<http://acmg.seas.harvard.edu/geos/>) of Sherwen et al. (2016) and Wang et al. (2021) (i.e., v10 and v12.9, respectively). These fields were generously provided by the respective authors of the two studies. They will be referred to as the Cl-Sherwen and Cl-Wang fields. Differences between the two fields are detailed below.

The last field was simulated by version 5.7b of the CCSR/NIES/FRCGC (Center for Climate System Research/National Institute for Environmental Studies/Frontier Research Center for Global Change) atmospheric GCM (Takigawa et al., 1999). This was provided by the GCP-GMB (Global Carbon Project - Global Methane Budget) team to run the inversions used in Saunio et al. (2020), although it was not mandatory. It is referred to as the Cl-Taki field.

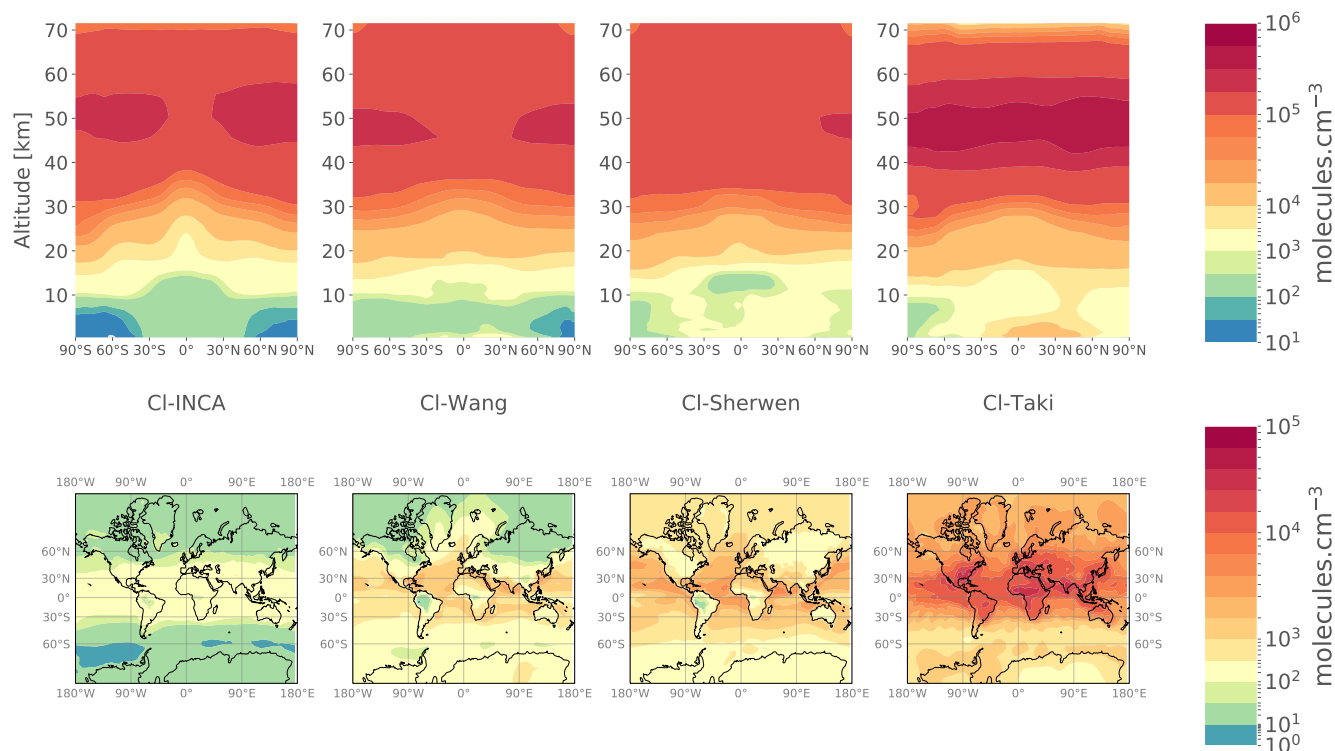


**Figure 1.** Annual mean meridional cross-section (upper panels) and tropospheric Cl concentrations (lower panels) for the four 3-D fields CI-INCA, CI-Wang, CI-Sherwen and CI-Taki.

150 In this study, we do not test the Cl fields from Hossaini et al. (2016) and Allan et al. (2007) because we want to carry out the sensitivity analysis while keeping a realistic and up-to-date range of concentrations. Their concentrations are indeed very likely to be overestimated (Gromov et al., 2018). Although Cl concentrations in the CI-Taki field are also very large, to our knowledge, CH<sub>4</sub> oxidation resulting from the prescription of this field has not been studied before. We therefore choose to include it here in order to quantify the associated sink and to illustrate the influence of such concentrations on CH<sub>4</sub> and

155  $\delta^{13}\text{C}(\text{CH}_4)$ .

The four fields are shown in Fig. 1. We use the lapse rate (2 K/km) definition from the World Meteorological Organization (WMO) and the meteorological fields from the online LMDz model to define the tropopause. Global mean tropospheric Cl concentrations range between 330 (CI-INCA) and 4730 (CI-Taki) molec.cm<sup>-3</sup>. The latitudinal distributions of tropospheric concentrations are similar, although CI-Wang, CI-Sherwen and CI-Taki have a greater spatial variability around their mean value than CI-INCA, especially in the mid-latitudes (75 %, 66 % and 63 % against 36 %, respectively). CI-Wang, CI-Sherwen and CI-INCA exhibits similar concentrations in the stratosphere ( $1.45 \pm 0.07 \times 10^5$  molec.cm<sup>-3</sup>). The increase in concentrations with altitude between the surface and 30 km is similar between all the fields, with a 0-30 km vertical gradient of  $4.4 \pm 1.0 \times 10^4$  molec.cm<sup>-3</sup>. Stratospheric concentrations are however larger in CI-Taki, reaching a mean value of  $2.1 \times 10^5$  molec.cm<sup>-3</sup>.



### 2.3 Description of simulations

165 Mole fractions of  $^{12}\text{CH}_4$  and  $^{13}\text{CH}_4$  are simulated over the 1998-2018 period. The distributions of OH and  $\text{O}(^1\text{D})$  have also been simulated with the LMDz-INCA model and are outputs of the same simulation that provided the Cl-INCA field. These OH and  $\text{O}(^1\text{D})$  fields are used in all simulations performed here.

Our SimREF reference simulation uses the Cl-Wang field as it is the most recent field and is taken from the most comprehensive study to date. In addition, we want our reference simulation to infer realistic  $\text{CH}_4$  and  $\delta^{13}\text{C}(\text{CH}_4)$  distributions with a good model-observation agreement. The fluxes and isotopic signatures of five emission categories used in this study therefore result from an atmospheric inversion over 1998-2018 based on a joint assimilation of  $\text{CH}_4$  and  $\delta^{13}\text{C}(\text{CH}_4)$  in the ClF-LMDz-SACS system designed by Thanwerdas et al. (2021). The inversion assimilates observations introduced in Sect. 2.4. The Cl-Wang field was not available when this inversion was launched. Therefore, we instead prescribed the Cl-INCA field and scaled the tropospheric mean Cl concentration ( $330 \text{ molec.cm}^{-3}$ ) to that of Wang et al. (2019) ( $620 \text{ molec.cm}^{-3}$ ), very similar to that of Wang et al. (2021) ( $630 \text{ molec.cm}^{-3}$ ). We acknowledge the small difference between the inversion setup and the reference scenario setup, due to small differences in Cl concentrations. However, using the optimized fluxes and signatures together with the prescribed sinks, a model-observation agreement (Root Mean Square Error) of 3.6 ppb for  $\text{CH}_4$  and 0.04 ‰ for  $\delta^{13}\text{C}(\text{CH}_4)$  is obtained on global averages, and is considered sufficient to validate the conclusions of this study. More information about the inversion is given in the supplement (Text S1). Emissions and source isotopic signatures are given in Table 2. Both vary over time and space and are prescribed as monthly fields at the horizontal resolution of the model.

The Cl-Sherwen, Cl-Taki and Cl-INCA fields presented in Sect. 2.2 are used in the SimSherwen, SimTaki and SimINCA simulations, respectively. In Saunois et al. (2020), the majority of inversions are performed without a tropospheric Cl sink; thus, we tested this with the SimNoTropo simulation where the Cl-Wang is used but with no Cl in the troposphere. Moreover, as LMDz-SACS completely omitted the Cl sink in previous studies, we estimate the errors generated by this omission running the SimNoCl simulation, which has no Cl sink. A summary of the simulations and their characteristics is provided in Table 3.

**Table 2.** Global  $\text{CH}_4$  emissions and associated flux-weighted isotopic signatures by source category. Given values are averages over 1998-2018. Numbers in brackets are minimum and maximum over this period of time [min/max].

Categories	$\text{CH}_4$ emissions ( $\text{TgCH}_4\cdot\text{yr}^{-1}$ )	Isotopic signature (‰ - VPDB)
Biofuels-Biomass Burning (BB)	28 [23 / 44]	-21.5 [-22.2 / -21.3]
Agriculture and Waste (AGW)	221 [197 / 241]	-58.3 [-59.4 / -57.0]
Fossil Fuels and Geological sources (FFG)	124 [101 / 142]	-43.5 [-44.8 / -42.1]
Natural sources apart from wetlands (NAT)	23 [23 / 23]	-50.8 [-50.8 / -50.8]
Wetlands (WET)	192 [184 / 202]	-56.6 [-56.6 / -56.5]
Total	588 [530 / 639]	-52.6 [-53.3 / -52.0]



**Table 3.** Nomenclature and description of the sensitivity tests.

Sensitivity test	Chemistry model	Field name	Modification
SimNoCl	None	None	None
SimNoTropo	GEOS-Chem v12.09 Wang et al. (2021)	Cl-Wang	No Cl in the troposphere
SimREF	GEOS-Chem v12.09 Wang et al. (2021)	Cl-Wang	None
SimINCA	LMDz-INCA	Cl-INCA	None
SimSherwen	GEOS-Chem v10 Sherwen et al. (2016)	Cl-Sherwen	None
SimTaki	CCSR/NIES/FRCGC AGCM v5.7b Takigawa et al. (1999)	Cl-Taki	None

## 2.4 Observations

Different datasets of observations are used to evaluate our simulations and to estimate the impact of the Cl field. These observations are of several types and could be assimilated in atmospheric inversions: surface measurements of CH<sub>4</sub> and  $\delta^{13}\text{C}(\text{CH}_4)$  as well as in situ vertical profiles of CH<sub>4</sub>.

190 CH<sub>4</sub> observations measured at 79 surface stations of the Global Greenhouse Gas Reference Network (GGGRN), part of the NOAA-ESRL's Global Monitoring Laboratory (NOAA GML), were used to perform the inversion introduced in Sect. 2.3. Reported uncertainties are generally below 5 ppb.  $\delta^{13}\text{C}(\text{CH}_4)$  measurements provided by the Institute of Arctic and Alpine Research (INSTAAR) by analyzing air samples collected at 22 stations on an approximately weekly basis were also assimilated (White et al., 2021). Reported uncertainties are generally below 0.15 ‰.

195 A total of 11 MBL sites (i.e., the site samples consist mainly of well-mixed MBL air) among those that recorded  $\delta^{13}\text{C}(\text{CH}_4)$  values over the 1998-2018 period were selected to sample simulated values at the time and locations of available observations. The station locations and additional information can be found in the supplementary Figure S3, Tables S5 and S6.

Finally, an analysis of the impact of Cl on CH<sub>4</sub> vertical profiles is conducted using a set of 115 AirCore profiles recovered from 11 different sites over the 2012-2018 period. A total of 80 profiles are provided by the NOAA GML aircraft programme (Baier et al., 2021; Karion et al., 2010) and 35 others by the French AirCore programme (Membrive et al., 2017). The balloon-borne AirCore technique (Karion et al., 2010) allows air samples to be taken from the stratosphere (up to approximately 30 km) to the ground, upon a parachute-based descent. Figure S4 and Table S4, in the supplement, provide information about the provider, location and number of profiles collected. Reported uncertainties generally increase with altitude due to end-member mixing within the AirCore samples. They are below 2 ppb in the troposphere and can reach 10 ppb in the lower  
205 stratosphere.



### 3 Results

#### 3.1 Quantification of the Cl sink

The simulated chemical sink of CH<sub>4</sub> due to Cl oxidation varies depending on the prescribed Cl field. We therefore obtain different sink intensities depending on the simulation. Table 4 summarizes the intensities of these sinks averaged over the simulation period in both the troposphere and stratosphere. Also included in the comparison are the tropospheric Cl sinks from Hossaini et al. (2016) and Allan et al. (2007), and the stratospheric Cl sink from Patra et al. (2011). All of them are used in many inversions. The Cl sink used in Patra et al. (2011), which is exclusively stratospheric, is the sum of O(<sup>1</sup>D) and Cl sinks. Contributions of O(<sup>1</sup>D) and Cl sinks to the stratospheric sink were previously estimated to be 20-40 % and 20-35 %, respectively (McCarthy et al., 2003; Rice et al., 2003). Using these estimates, the Cl sink from Patra et al. (2011) should contribute between 1.3 % and 2.6 % of the total sink. Using our own estimates of O(<sup>1</sup>D) concentrations, we obtain a Cl contribution of 2.6 %.

From our simulations, contributions from the tropospheric Cl sink with Cl-Wang (0.6 %) and Cl-Sherwen (1.8 %) are slightly lower than those given in the associated papers (i.e., 0.8 % and 2 %, respectively). This discrepancy is likely due to a slight difference in the definition of the tropopause level or/and in the prescribed OH sink that is used to calculate the total chemical sink.

The tropospheric sink provided by Allan et al. (2007) is well above the other recent values. The tropospheric value from Hossaini et al. (2016), used in recent studies (Saunois et al., 2020; McNorton et al., 2018), is also slightly above that of Cl-Sherwen (Table 4: 1.4 times higher) but well above that of Cl-Wang and Cl-INCA (4 and 8.5 times higher). In the troposphere, the sink induced by Cl-Taki is much larger than the other sinks (up to 28 times larger) and therefore even larger than the value suggested by Allan et al. (2007) which is very likely to be overestimated (Gromov et al., 2018). In the stratosphere, the sink is also slightly larger (1.3 times that of Cl-Sherwen).

Apart from the Cl-Taki field, we selected here only the fields that provided a realistic range of concentrations when applying the conclusions of Gromov et al. (2018). We therefore consider only the Cl fields that give a CH<sub>4</sub> tropospheric oxidation below 2 % as realistic. These fields happen to be the most recent and up-to-date estimations. In the stratosphere, all tested fields are considered realistic because they provide an oxidation between 1.1 and 1.6 %, therefore in agreement with Saunois et al. (2020) and McCarthy et al. (2003) (0.4-2.4 %). In the following analysis, results from SimTaki are presented only to illustrate why a Cl field should be rigorously analyzed (concentration, oxidation) before prescribing it in a forward or inverse simulation.

#### 3.2 CH<sub>4</sub> surface concentrations

The impact of the Cl sink on CH<sub>4</sub> mole fractions is analyzed by comparing the simulations against SimREF at MBL station locations providing δ<sup>13</sup>C(CH<sub>4</sub>) data. Since the Cl fields vary mainly as a function of latitude, the comparisons are made by averaging values over bands of latitude. Here, the bias *b* is defined as :

$$b_{X,i,l} = \overline{X_{i,s}} - X_{\text{SimREF},s} \quad (2)$$



**Table 4.** Percentage of contribution from Cl oxidation to total chemical oxidation (Cl, O(<sup>1</sup>D) and OH) and sink intensity. Values are given for the tropospheric, stratospheric and total (tropospheric + stratospheric) Cl sinks for several fields, either used in the simulations or in other studies. \* Values taken from literature. H16 : Hossaini et al. (2016) ; A07 : Allan et al. (2007) ; P11 : Patra et al. (2011)

Field	Troposphere			Stratosphere			Total	
	Oxidation (%)	Sink (TgCH <sub>4</sub> .yr <sup>-1</sup> )	Conc. (molec.cm <sup>-3</sup> )	Oxidation (%)	Sink (TgCH <sub>4</sub> .yr <sup>-1</sup> )	Conc. (molec.cm <sup>-3</sup> )	Oxidation (%)	Sink (TgCH <sub>4</sub> .yr <sup>-1</sup> )
SimNoCl	0	0	0	0	0	0	0	0
SimNoTropo	0	0	0	1.1	6.1	1.5 × 10 <sup>5</sup>	1.1	6.1
SimINCA	0.3	1.5	3.3 × 10 <sup>2</sup>	1.0	5.2	1.4 × 10 <sup>5</sup>	1.2	6.7
SimREF	0.6	3.2	6.1 × 10 <sup>2</sup>	1.1	6.1	1.5 × 10 <sup>5</sup>	1.7	9.3
SimSherwen	1.8	9.9	1.1 × 10 <sup>3</sup>	1.2	6.4	1.6 × 10 <sup>5</sup>	3.0	16.3
H16*	2.6	12-13	1.3 × 10 <sup>3</sup>	N/A	N/A	N/A	N/A	N/A
A07*	5	25	N/A	N/A	N/A	N/A	N/A	N/A
SimTaki	8.5	47.0	4.7 × 10 <sup>3</sup>	1.6	9.0	2.1 × 10 <sup>5</sup>	10.1	56.0
P11*	N/A	N/A	N/A	1.3-2.6	6.8-13.7	N/A	N/A	N/A

where  $b_{X,i,l}$  is the bias for a specific quantity  $X$  (i.e., CH<sub>4</sub> or  $\delta^{13}\text{C}(\text{CH}_4)$ ), a specific simulation  $i$ , and a specific band of latitude  $l$ .  $X_{i,s}$  denotes the CH<sub>4</sub> or  $\delta^{13}\text{C}(\text{CH}_4)$  values simulated by a simulation  $i$  and at a station  $s$ . The  $(\bar{\cdot})^l$  symbol indicates the mean over all the stations whose location is inside the band of latitude  $l$ .

In a box model, the temporal evolution of the CH<sub>4</sub> budget for a simulation  $i$  is described by the equation below :

$$\frac{dB_i}{dt} = S - \frac{B_i}{\tau_i} \quad (3)$$

where  $B_i$  is the mass of CH<sub>4</sub> in the atmosphere in TgCH<sub>4</sub>,  $S$  is the source in TgCH<sub>4</sub>.yr<sup>-1</sup> and  $\tau_i$  is the chemical lifetime of CH<sub>4</sub> in the atmosphere in yr. Note that the same sources are prescribed for all simulations. The temporal evolution of the CH<sub>4</sub> budget is not linear, because the sink is proportional to CH<sub>4</sub> mole fractions. CH<sub>4</sub> decrease/increase induces a negative feedback on the magnitude of the sink, leading to a stabilization of the mass of CH<sub>4</sub> after several decades if  $S$  and  $\tau_i$  are constant over time. Here, the bias between two simulations is caused by a change in  $\tau$  because we modify the Cl field. The evolution of the bias  $b$  can therefore be described by the equation :

$$\frac{db}{dt} = \frac{d(B_2 - B_1)}{dt} = -\frac{B_1}{\tau_1} + \frac{B_2}{\tau_2} \quad (4)$$

However, in a surface-based inversion (i.e., an inversion assimilating observations from surface stations) without sink optimization, the bias is compensated by a correction of the CH<sub>4</sub> global surface flux  $S + \Delta S$ . The inversion system therefore answers the question : "What is the value of  $\Delta S$  that will offset the bias caused by a change in the prescribed sink ?". The temporal evolution of the bias between a simulation and the reference simulation can therefore be described by the equation :

$$\frac{db}{dt} = \Delta S - \frac{b}{\tau_{ref}} \quad (5)$$

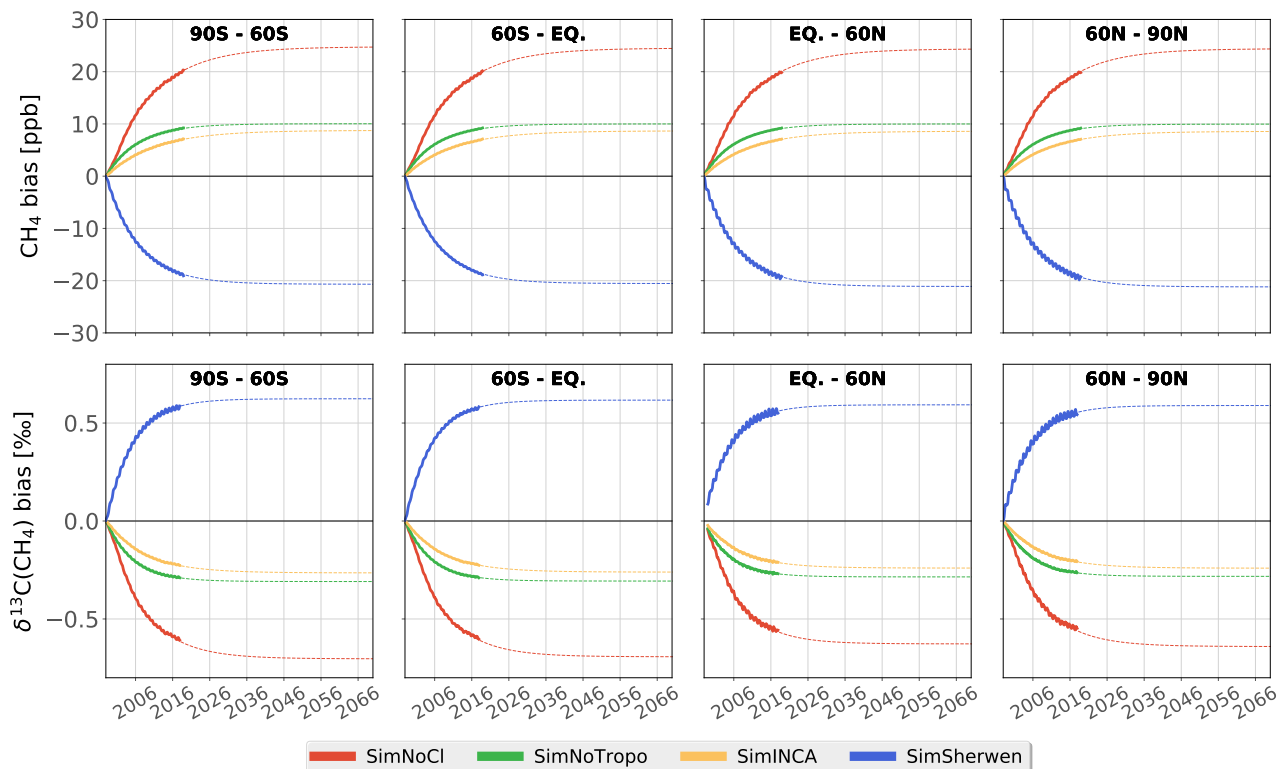


**Figure 2.** CH<sub>4</sub> and  $\delta^{13}\text{C}(\text{CH}_4)$  biases averaged over bands of latitude. Solid lines are the monthly simulated values and dashed lines are the extended values following the methods from Sect. 3.2.

255  $\tau_{ref}$  denotes the chemical lifetime in the reference simulation. We consider that  $\Delta S$  is constant over time as the inter-annual  
 variability of the Cl sink is below  $0.4 \text{ TgCH}_4.\text{yr}^{-1}$ . In that case, the solution of this equation is :

$$b(t) = \Delta S \times \tau_{ref} \times \left(1 - e^{-\frac{t}{\tau_{ref}}}\right) \quad (6)$$

The value of  $\Delta S$  can be obtained by analyzing the temporal evolution of the bias and, in particular, by looking at the value of  
 the bias when it is stabilized (steady state). Here, after 21 years of simulation, the stabilization is not reached yet (see Fig. 2,  
 260 top row). Therefore, we choose to extend our results by applying a curve fitting function to our simulated values :

$$b_{X,i,l}(t) = A_{X,i,l} \times B_{X,i,l} \times \left(1 - e^{-\frac{t}{B_{X,i,l}}}\right) \quad (7)$$

$A_{X,i,l}$  and  $B_{X,i,l}$  are two constants that the curve fitting algorithm returns in order to maximize the agreement between the simu-  
 lated values and the curve fitting function. Using this function, the results are extended until 2070 to reach a clear stabilization  
 of simulated biases (see Fig. 2, top row). 

265 At steady state, the bias of CH<sub>4</sub> at the surface varies between -20.0 ppb for SimSherwen and 24.5 ppb for SimNoCl (Table  
 5, second column). An estimation of  $\Delta S$  is given by the coefficient  $A_{X,i,l}$ . It provides a result in  $\text{ppb}.\text{yr}^{-1}$ . To convert this value



in  $\text{TgCH}_4.\text{yr}^{-1}$ , we use a conversion factor of  $2.767 \text{ Tg.ppb}^{-1}$  (Lassey et al., 2000) and show the final estimates in Table 5, fourth column. For SimNoCl and SimSherwen, these estimations are very close (difference of less than  $0.2 \text{ TgCH}_4.\text{yr}^{-1}$ ) to the tropospheric Cl sink discrepancies from Table 4. Indeed, as the stratospheric Cl sinks in SimREF, SimINCA, SimNoTropo and SimSherwen are almost identical, the biases induced by tropospheric Cl sink discrepancies will be logically compensated by a source adjustment of the same intensity as the sink discrepancy. For SimNoCl, the biases at the surface are also influenced by large stratospheric sink discrepancies. Therefore, the inferred adjustment values cannot be so simply related to the sink discrepancies. Also, latitude has a very low influence on biases and adjustment values, causing a variation of less than 5 % around the mean value (see Fig. 2).

We conclude that a source adjustment of  $12.3 \text{ TgCH}_4.\text{yr}^{-1}$  would be necessary between a surface-based inversion without Cl sink, such as the inversions carried out with LMDz-SACS up to now, and a surface-based inversion adopting the Cl-Sherwen field. Saunois et al. (2020) obtained an uncertainty on the total  $\text{CH}_4$  fluxes of about  $40 \text{ TgCH}_4.\text{yr}^{-1}$  (maximum - minimum difference) across the different top-down inversions reported. The difference in the Cl configuration between the multiple inversions of Saunois et al. (2020) may have contributed to the uncertainty they estimated. Although the adjustment value we obtain here thus remains lower than the uncertainty generated by the different configurations used in Saunois et al. (2020), it is not negligible as we make the point that this source adjustment could be much larger if an unrealistic Cl field was used. For example, prescribing the Cl-Taki field instead of the Cl-Wang field would result in an adjustment value of  $48.1 \text{ TgCH}_4.\text{yr}^{-1}$ . If a single Cl configuration for all inversions could be agreed upon, this would likely lead to a reduction of the uncertainty on emission fluxes.

**Table 5.** Global adjustment values of  $\text{CH}_4$  source and isotopic signatures inferred from  $\text{CH}_4$  and  $\delta^{13}\text{C}(\text{CH}_4)$  biases at the surface. Second column is the global  $\text{CH}_4$  bias at the surface and at steady state. Third column is the global  $\delta^{13}\text{C}(\text{CH}_4)$  bias at the surface and at steady state. Fourth column is the global  $\text{CH}_4$  source adjustment value estimated using the methods described in Sect. 3.2. Fifth column is the  $\delta^{13}\text{C}(\text{CH}_4)_{\text{source}}$  adjustment value estimated using the methods described in Sect. 3.3. Latitudinal dependency is reported as a minimum-maximum range [min/max] for all values.

Simulation	Bias		Source adjustment	
	$\text{CH}_4$ (ppb)	$\delta^{13}\text{C}(\text{CH}_4)$ (‰)	Flux ( $\text{TgCH}_4.\text{yr}^{-1}$ )	Signature (‰)
SimNoCl	24.5 [24.4 / 24.8]	-0.66 [-0.70 / -0.63]	-5.7 [-5.7 / -5.7]	0.66 [0.63 / 0.70]
SimNoTropo	10.0 [10.0 / 10.0]	-0.30 [-0.31 / -0.28]	-3.2 [-3.2 / -3.2]	0.30 [0.28 / 0.31]
SimINCA	8.6 [8.6 / 8.8]	-0.25 [-0.26 / -0.24]	-1.9 [-2.0 / -1.9]	0.25 [0.24 / 0.26]
SimSherwen	-20.0 [-21.2 / -20.5]	0.60 [0.59 / 0.62]	6.6 [6.5 / 6.8]	-0.60 [-0.62 / -0.59]
SimTaki	-140.1 [-142.2 / -138.2]	4.13 [4.01 / 4.24]	48.1 [46.9 / 49.2]	-4.13 [-4.24 / -4.01]



### 285 3.3 $\delta^{13}\text{C}(\text{CH}_4)$ signal at the surface

In contrast with the  $\text{CH}_4$  biases, the  $\delta^{13}\text{C}(\text{CH}_4)$  biases between the simulations are much larger than recent  $\delta^{13}\text{C}(\text{CH}_4)$  observed downward shifts ( $\sim 0.3 \text{‰}$  since 2007). We use the same curve fitting method as before to propagate the time-series until 2070 in order to reach a steady state (see Fig. 2, bottom row).

SimNoTropo, SimINCA, SimREF and SimSherwen have very similar stratospheric Cl sinks (Table 4). Therefore, biases  
290 for SimNoCl, SimNoTropo, and SimSherwen are mostly generated by discrepancies in tropospheric Cl sink intensity. We can estimate that each percent increase in how much  $\text{CH}_4$  is oxidized by Cl leads to an additional  $0.53 \text{‰}$  increase in  $\delta^{13}\text{C}(\text{CH}_4)$ , therefore larger than the global downward shift observed since 2007. After 14 years of simulation, we obtain a value of  $0.46 \text{‰}$ , very close to the value of  $0.5 \text{‰}$  inferred by Strode et al. (2020) after the same number of years.

Stratospheric Cl also influences  $\delta^{13}\text{C}(\text{CH}_4)$  at the surface through STE. We estimate this influence using the bias between  
295 SimNoCl and SimNoTropo. Intrusions of stratospheric air are therefore responsible of an enrichment at the surface stations of  $0.30 \pm 0.01 \text{‰}$  (depending on the latitude) after 21 years of simulation, larger than the value of Wang et al. (2002) inferred between 1970 and 1992 ( $0.23 \text{‰}$ ).

To reduce these biases to zero, an inversion system would adjust the globally-averaged isotopic signature of the  $\text{CH}_4$  sources, denoted by  $\delta^{13}\text{C}(\text{CH}_4)_{\text{source}}$ . This adjustment factor would be roughly equal to the opposite of the bias at steady state (see  
300 demonstration in the supplementary Text S2). It would therefore oscillate between  $-0.60 \text{‰}$  (SimSherwen) and  $+0.66 \text{‰}$  (SimNoCl) around the mean isotopic signature of the global  $\text{CH}_4$  source prescribed in SimREF. We would therefore obtain, after the inversion process, a mean global signature between  $-53.20 \text{‰}$  (SimSherwen) and  $-51.94 \text{‰}$  (SimNoCl).

The system would modify  $\delta^{13}\text{C}(\text{CH}_4)_{\text{source}}$  by changing the source mixture and/or the isotopic signatures of the multiple emission categories, with a weight depending on uncertainties associated to both. For instance, an adjustment of  $-0.60 \text{‰}$   
305 could be made by increasing the wetlands share from 32 % to 43 % or by shifting the mean isotopic signature of wetlands from  $-56.6$  to  $-58.5 \text{‰}$ , more in agreement with recent estimates (Ganesan et al., 2018; Sherwood et al., 2017) than our inverted value (see Table 2). However, the system would likely change not only wetlands but all emission categories, possibly limiting an unlikely large change in wetlands emissions only. Nevertheless, the configuration used to represent the Cl sink could largely influence the result of an inversion assimilating both  $\text{CH}_4$  and  $\delta^{13}\text{C}(\text{CH}_4)$ .

### 310 3.4 $\text{CH}_4$ and $\delta^{13}\text{C}(\text{CH}_4)$ seasonal cycles

To investigate the seasonal cycle, the simulations are compared against SimREF by averaging values over latitudinal bands (see Fig. 3) as in Sect. 3.2 and 3.3.

With the realistic Cl fields tested here, the influence on the  $\text{CH}_4$  seasonal cycle is negligible regardless of the latitudinal band analyzed. The variation in the seasonal cycle amplitude due to Cl is about  $0.4 \text{ ppb}$  whereas the seasonal cycle amplitude is  
315 about  $20 \text{ ppb}$  in the Southern Hemisphere and  $30 \text{ ppb}$  in the Northern Hemisphere. The variation therefore accounts for 1-2 % of the seasonal cycle amplitude.

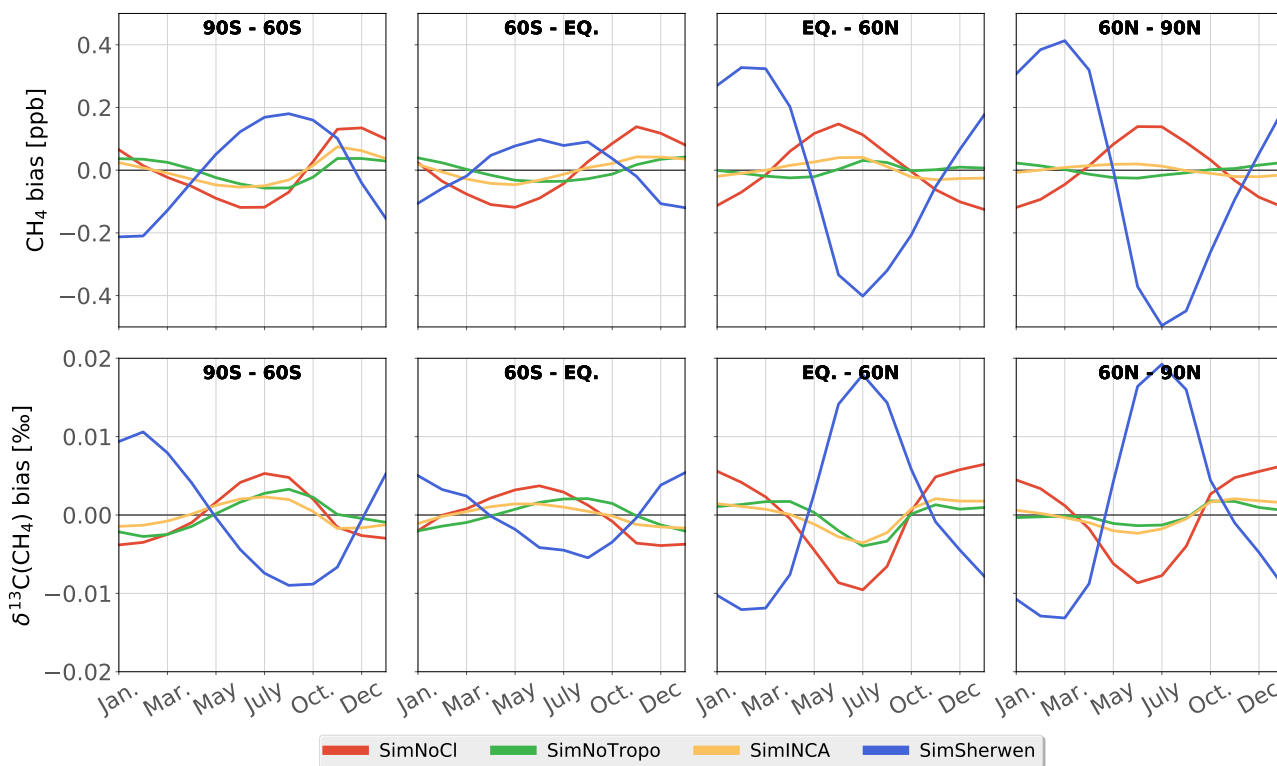


**Figure 3.** Seasonal cycles of  $\text{CH}_4$  and  $\delta^{13}\text{C}(\text{CH}_4)$  biases between the surface values simulated by the various simulations (see Sect. 2.3) and those simulated by SimREF. The biases are averaged over four bands of latitude.

The impact is more important for the  $\delta^{13}\text{C}(\text{CH}_4)$  seasonal cycle and is dependent on latitude. In the Southern Hemisphere, the variation in amplitude between SimREF and SimSherwen is about 0.02 ‰, which represents 20 % of the total seasonal cycle amplitude. In the Northern Hemisphere, the variation can exceed 0.03 ‰, which represents 10 % of the seasonal cycle amplitude.

SimTaki (not shown on Fig. 3 for clarity reason) causes a much larger variation in seasonal cycle for both  $\text{CH}_4$  and  $\delta^{13}\text{C}(\text{CH}_4)$ . For  $\text{CH}_4$ , variations reach 5 % in the Southern Hemisphere and 10 % in the Northern Hemisphere. As for  $\delta^{13}\text{C}(\text{CH}_4)$ , variations go up to 99 % in the Southern Hemisphere and 58 % in the Northern Hemisphere.

The influence of Cl on  $\delta^{13}\text{C}(\text{CH}_4)$  seasonal cycle must be considered as it will impact the results of an inversion with  $\delta^{13}\text{C}(\text{CH}_4)$  data assimilation. A misrepresentation of the seasonal cycle forces the system to adjust the intensity of sources that actively participate in the seasonal cycle, such as wetlands or biomass burning emissions. This influence is negligible for  $\text{CH}_4$  and noticeable for  $\delta^{13}\text{C}(\text{CH}_4)$  when keeping realistic Cl concentrations but becomes very large when using other Cl fields, such as the Cl-Taki field.



### 3.5 CH<sub>4</sub> vertical profiles

330 Vertical profile measurements of CH<sub>4</sub> are too scarce to be considered as a stand-alone constraint in inversion systems, and so are rather used as evaluation data. Nevertheless, as their accuracy, spatial coverage and number increase, their assimilation will become increasingly relevant. It is, however, necessary to increase the model-observation agreement, especially in the stratosphere, before considering their assimilation. We analyze here the influence of the CI configuration on these profiles. We also compare the simulated vertical profiles to observations to investigate whether modifying the CI configuration can help to  
 335 reduce the model-observation discrepancies.

Simulated vertical profiles are sampled at the same locations and time as the observations available. The bias  $b_{X,y,p,d_1,d_2}$  between two vertical profiles  $d_1$  and  $d_2$  (simulated or observed) for a specific profile  $p$ , a specific quantity  $X$  (i.e., CH<sub>4</sub>) and a specific layer  $y$  (troposphere, stratosphere or total) is given by:

$$b_{X,y,p,d_1,d_2} = \overline{X_{d_1,p} - X_{d_2,p}}^y \quad (8)$$

340 The  $(\overline{\cdot})^y$  symbol indicates the mean over all the vertical levels in the layer  $y$ . We also define the mean bias as the bias averaged over all available vertical profiles :

$$\bar{b}_{X,y,d_1,d_2} = \overline{b_{X,y,p,d_1,d_2}}^p \quad (9)$$

**Table 6.** Mean bias relative to SimREF for CH<sub>4</sub> vertical profiles in the troposphere and stratosphere as well as in the Northern and Southern Hemisphere.

	Troposphere		Stratosphere	
	Northern Hemisphere	Southern Hemisphere	Northern Hemisphere	Southern Hemisphere
Simulation	ppb			
SimNoCl	19.3	19.1	50.8	38.9
SimNoTropo	10.9	10.8	15.2	12.9
SimINCA	6.8	6.7	11.8	9.2
SimSherwen	-18.7	-18.2	-18.1	-17.9
SimTaki	-129.7	-125.0	-118.5	-121.4

The mean bias relative to SimREF is given for all simulations and observations in Table 6. A change in the CI field (and keeping it realistic) induces a maximum mean bias of 51 ppb in the stratosphere (SimNoCl). For all simulations besides  
 345 SimNoCl, the bias is roughly constant over the entire column (see Fig. 4), because the CI concentrations in the stratosphere are very similar. Also, a change in the tropospheric CI sink influences tropospheric and stratospheric values to the same magnitude. For SimNoCl, the bias is constant in the troposphere but starts increasing above 15 km at 7.5 ppb.km<sup>-1</sup> in the Northern Hemisphere and 7 ppb.km<sup>-1</sup> in the Southern Hemisphere. At 25 km, the bias therefore reaches 130 ppb in the Northern Hemisphere for this simulation.



350 Model-observation discrepancies reaches 250 ppb (around 20 and 25 km) in both Hemispheres. Root Mean Square Error (RMSE) in the stratosphere is  $102 \pm 21$  ppb in the Northern Hemisphere and  $84 \pm 15$  ppb in the Southern Hemisphere for SimREF. For all simulations, inflections of mole fractions observed at 15 and 20 km in the Northern Hemisphere are simulated 5 km higher ( $\sim 20$  and 25 km) than observed. These misrepresentations lead to simulated vertical gradients between 15 and 25 km much stronger than observed (900 ppb against 650 ppb in the Northern Hemisphere). Unfortunately, modifying the  
355 prescribed Cl field does not correct these errors.

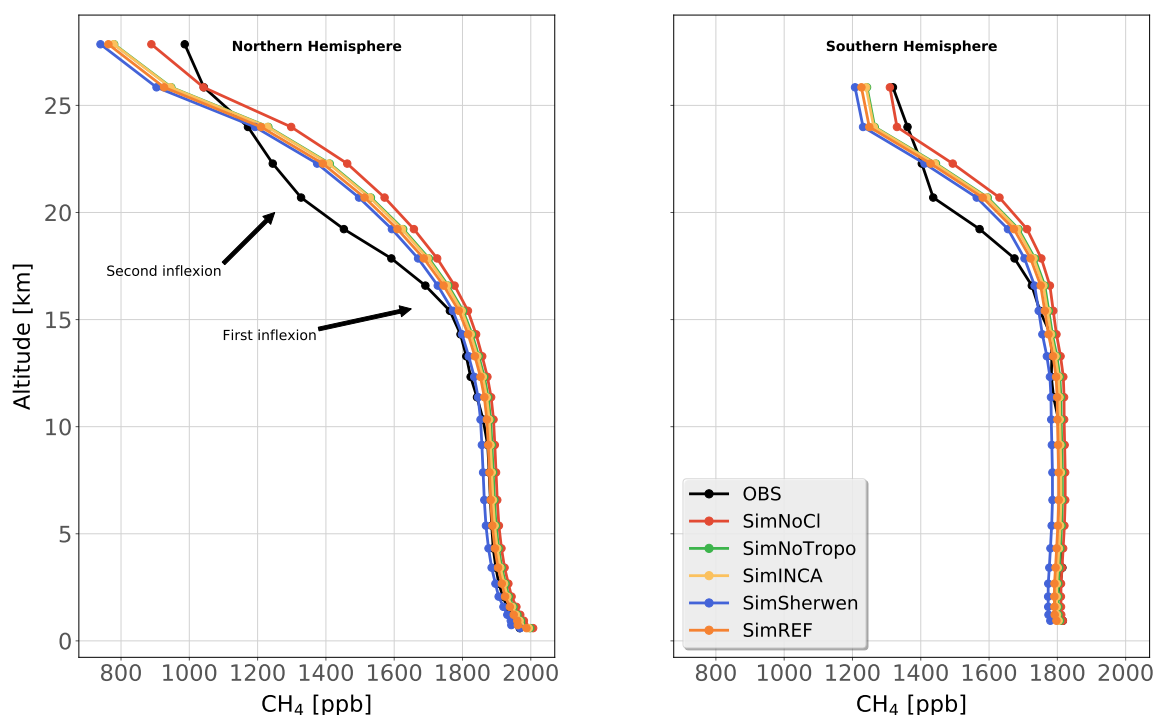


**Figure 4.** Observed and simulated CH<sub>4</sub> vertical profiles for the Northern Hemisphere (left panel) and Southern Hemisphere (right panel). All available vertical profiles have been averaged.

Although modifying the prescribed Cl field can induce local differences in stratospheric mole fractions of the same order of magnitude as the model errors, none of the tested Cl sink really improves our model-observation agreement in the stratosphere as the inflections of mole fractions are not properly represented. Patra et al. (2011) already mentioned that strong vertical gradients of CH<sub>4</sub> around the tropopause may be caused by a too slow Brewer-Dobson circulation so these discrepancies are  
360 possibly due to transport errors rather than errors in removal rates. Further investigating the discrepancy in the stratosphere is however beyond the scope of this study.





Ostler et al. (2016) showed that model errors in simulating stratospheric CH<sub>4</sub> contribute to model biases when compared to observed column-averaged CH<sub>4</sub> dry-air mole fractions (XCH<sub>4</sub>) from the Total Carbon Column Observing Network (TCCON). XCH<sub>4</sub> obtained by remote sensing techniques are now massively assimilated in inversions because satellite observations offer a much larger spatial coverage than in situ measurements. Rigorously estimating the influence of Cl concentrations on a satellite-based inversion would require more than an one-box model approximation. We therefore include only a simple analysis using data from the GOSAT satellite in the supplementary Text S3.

#### 4 Conclusions

In this study, we tested multiple Cl fields suggested by recent studies to investigate the influence of the Cl configuration on CH<sub>4</sub> and  $\delta^{13}\text{C}(\text{CH}_4)$ , and to estimate its potential impact on the estimation of CH<sub>4</sub> sources and isotopic signatures with top-down approaches.

We tested a realistic range of Cl concentrations, i.e., resulting in Cl tropospheric and stratospheric oxidations that are in agreement with recently published studies. We also included a Cl field suggested by the GCP 2018 protocol to be prescribed in inverse simulations in order to investigate its influence on CH<sub>4</sub> and  $\delta^{13}\text{C}(\text{CH}_4)$  values in comparison with more realistic and recent Cl fields. The realistic Cl fields tested here are responsible for between 0.3 % and 1.8 % of the total CH<sub>4</sub> sink in the troposphere and between 1.0 % and 1.2 % in the stratosphere.

At the surface, the change in the Cl field and thus in the associated CH<sub>4</sub> sink results in a bias in CH<sub>4</sub> mole fractions that reaches a maximum value of 44.5 ppb at steady state. An inversion system would adjust the CH<sub>4</sub> surface fluxes by a value of 12.3 TgCH<sub>4</sub>.yr<sup>-1</sup> to compensate for these biases. This adjustment remains small in comparison to the uncertainties inferred by Saunio et al. (2020). However, the use of perhaps more unrealistic Cl fields (as suggested by recent literature) can generate much larger biases.

$\delta^{13}\text{C}(\text{CH}_4)$  values at the surface are also shifted by a change in the prescribed Cl field. In particular, we find an increase in the  $\delta^{13}\text{C}(\text{CH}_4)$  global mean at the surface of 0.53 ‰ at the surface for each additional percent of contribution from the tropospheric Cl sink to the total CH<sub>4</sub> sink. In an inversion, this additional percent of contribution would reduce the inferred globally-averaged isotopic signature by 0.53 ‰. Also, we find that intrusions of stratospheric air are responsible for an enrichment of  $\delta^{13}\text{C}(\text{CH}_4)$  by 0.30 ‰ at the surface between 1998 and 2018. Neglecting the influence of stratospheric Cl on  $\delta^{13}\text{C}(\text{CH}_4)$  surface values could therefore increase the global mean isotopic signature estimated by an inversion by 0.30 ‰.

CH<sub>4</sub> seasonal cycles are only slightly influenced by a modification of the Cl sink (1-2 % change in the seasonal cycle amplitude). Changing the Cl field can nevertheless modify the amplitudes of  $\delta^{13}\text{C}(\text{CH}_4)$  seasonal cycle by up to 10-20 ‰, depending on the latitude.

We also investigate the influence of Cl concentrations on the modeling of vertical profiles. We find that stratospheric model-observation discrepancies in LMDz-SACS are unlikely to be caused by a misrepresentation of the Cl sink, although a change in Cl concentrations can shift CH<sub>4</sub> mole fractions at 25 km by up to 130 ppb. Also, a change in the tropospheric Cl sink influences tropospheric and stratospheric CH<sub>4</sub> mole fractions to the same magnitude.



395 It is difficult to conclude which Cl field provides the most realistic representation of the Cl sink among those tested here. Recent developments and efforts have nevertheless narrowed the range of uncertainties regarding the Cl concentrations (less than  $1.1 \times 10^3$  molec.cm<sup>-3</sup> in the troposphere and  $1.4\text{-}1.6 \times 10^5$  molec.cm<sup>-3</sup> in the stratosphere). Our study shows that the impact of a change in Cl field on top-down CH<sub>4</sub> flux estimates should be small compared to current uncertainties in Saunois et al. (2020) if this change is made within a realistic range of Cl concentrations both in the troposphere and the stratosphere. A  
400 Cl configuration for all inversions agreed upon in multi-model studies such as Saunois et al. (2020) should however reduce the spread in estimated CH<sub>4</sub> emission fluxes. We show that the choice of the Cl field is however critical (both in the troposphere and the stratosphere) for the global estimates of an inversion assimilating  $\delta^{13}\text{C}(\text{CH}_4)$  observations and can lead to radically different source mixtures and/or source signatures.

*Data availability.* The data for CH<sub>4</sub> and  $\delta^{13}\text{C}(\text{CH}_4)$  observations were downloaded from the NOAA-ESRL server [https://www.esrl.noaa.gov/gmd/aftp/data/trace\\_gases](https://www.esrl.noaa.gov/gmd/aftp/data/trace_gases). Datasets for the input emissions were provided by the Global Carbon Project (GCP) team. Satellite data  
405 were provided by the corresponding author of Parker et al. (2020). The AirCore vertical profiles from the NOAA-ESRL Aircraft Program (DOI: 10.15138/6AV0-MY81, Version: 20181101) were provided by CS and BB. The Cl-Sherwen and Cl-Wang fields were provided by the corresponding authors of Sherwen et al. (2016) and Wang et al. (2021), respectively. The Cl-INCA field, the modeling output files and the AirCore vertical profiles from the French AirCore Program are available upon request from the corresponding author.

410 *Author contributions.* JT designed and run the simulation experiments and performed the data analysis presented in this paper. DH provided the Cl-INCA field used for the simulations. MS provided the CH<sub>4</sub> fluxes. MS, AB, IP and PB provided scientific and technical expertise. They also contributed to the scientific analysis of this work. JT prepared the manuscript with contributions from all co-authors.

*Competing interests.* The authors declare that they have no conflict of interest.

*Acknowledgements.* This work was supported by the CEA (Commissariat à l'Énergie Atomique et aux Énergies Alternatives). The study  
415 extensively relies on the meteorological data provided by the ECMWF. Calculations were performed using the computing resources of LSCE, maintained by François Marabelle and the LSCE IT team. The authors wish to thank the measurement teams from the NOAA GML and from INSTAAR for their work.



## References

- Allan, W., Struthers, H., and Lowe, D. C.: Methane carbon isotope effects caused by atomic chlorine in the marine bound-  
420 ary layer: Global model results compared with Southern Hemisphere measurements, *Journal of Geophysical Research*, 112,  
<https://doi.org/10.1029/2006JD007369>, 2007.
- Baier, B., Sweeney, C., T., N., Higgs, J., Wolter, S., and Laboratory, N. G. M.: NOAA AirCore atmospheric sampling system profiles (Version  
20181101) [Data set], NOAA GML, <https://doi.org/10.15138/6AV0-MY81>, 2021.
- Bousquet, P., Ciais, P., Miller, J. B., Dlugokencky, E. J., Hauglustaine, D. A., Prigent, C., Van der Werf, G. R., Peylin, P., Brunke, E.-G.,  
425 Carouge, C., Langenfelds, R. L., Lathière, J., Papa, F., Ramonet, M., Schmidt, M., Steele, L. P., Tyler, S. C., and White, J.: Contribution of  
anthropogenic and natural sources to atmospheric methane variability, *Nature*, 443, 439–443, <https://doi.org/10.1038/nature05132>, 2006.
- Burkholder, J. B., Abbatt, J. P. D., Huie, R. E., Kurylo, M. J., Wilmouth, D. M., Sander, S. P., Barker, J. R., Kolb, C. E., Orkin, V. L., and  
Wine, P. H.: JPL Publication 15-10: Chemical Kinetics and Photochemical Data for Use in Atmospheric Studies, p. 1392, 2015.
- Cantrell, C. A., Shetter, R. E., McDaniel, A. H., Calvert, J. G., Davidson, J. A., Lowe, D. C., Tyler, S. C., Cicerone, R. J., and Greenberg,  
430 J. P.: Carbon kinetic isotope effect in the oxidation of methane by the hydroxyl radical, *Journal of Geophysical Research: Atmospheres*,  
95, 22 455–22 462, <https://doi.org/https://doi.org/10.1029/JD095iD13p22455>, 1990.
- Chevallier, F., Fisher, M., Peylin, P., Serrar, S., Bousquet, P., Bréon, F.-M., Chédin, A., and Ciais, P.: Inferring CO<sub>2</sub>  
sources and sinks from satellite observations: Method and application to TOVS data, *Journal of Geophysical Research*, 110,  
<https://doi.org/10.1029/2005JD006390>, 2005.
- 435 Craig, H.: Isotopic standards for carbon and oxygen and correction factors for mass-spectrometric analysis of carbon dioxide, *Geochimica et*  
*Cosmochimica Acta*, 12, 133–149, [https://doi.org/10.1016/0016-7037\(57\)90024-8](https://doi.org/10.1016/0016-7037(57)90024-8), 1957.
- Dlugokencky, E. J.: NOAA/GML, [www.esrl.noaa.gov/gmd/ccgg/trends\\_ch4/](http://www.esrl.noaa.gov/gmd/ccgg/trends_ch4/), last access : 12 July 2021, 2021.
- Etheridge, D. M., Steele, L. P., Francey, R. J., and Langenfelds, R. L.: Atmospheric methane between 1000 A.D. and present: Ev-  
idence of anthropogenic emissions and climatic variability, *Journal of Geophysical Research: Atmospheres*, 103, 15 979–15 993,  
440 <https://doi.org/10.1029/98JD00923>, 1998.
- Fletcher, S. E. M., Tans, P. P., Bruhwiler, L. M., Miller, J. B., and Heimann, M.: CH<sub>4</sub> sources estimated from atmospheric observations of  
CH<sub>4</sub> and its <sup>13</sup>C/<sup>12</sup>C isotopic ratios: 2. Inverse modeling of CH<sub>4</sub> fluxes from geographical regions, *Global Biogeochemical Cycles*, 18,  
<https://doi.org/10.1029/2004GB002224>, 2004.
- Folberth, G. A., Hauglustaine, D. A., Lathière, J., and Brocheton, F.: Interactive chemistry in the Laboratoire de Météorologie Dynamique  
445 general circulation model: model description and impact analysis of biogenic hydrocarbons on tropospheric chemistry, *Atmospheric*  
*Chemistry and Physics*, 6, 2273–2319, <https://doi.org/10.5194/acp-6-2273-2006>, 2006.
- Fujita, R., Morimoto, S., Maksyutov, S., Kim, H.-S., Arshinov, M., Brailsford, G., Aoki, S., and Nakazawa, T.: Global and Regional CH<sub>4</sub>  
Emissions for 1995–2013 Derived From Atmospheric CH<sub>4</sub>, δ<sup>13</sup>C-CH<sub>4</sub>, and δD-CH<sub>4</sub> Observations and a Chemical Transport Model,  
*Journal of Geophysical Research: Atmospheres*, 125, e2020JD032 903, <https://doi.org/https://doi.org/10.1029/2020JD032903>, 2020.
- 450 Ganesan, A. L., Stell, A. C., Gedney, N., Comyn-Platt, E., Hayman, G., Rigby, M., Poulter, B., and Hornibrook, E. R. C.:  
Spatially Resolved Isotopic Source Signatures of Wetland Methane Emissions, *Geophysical Research Letters*, 45, 3737–3745,  
<https://doi.org/10.1002/2018GL077536>, 2018.
- Gromov, S., Brenninkmeijer, C. A. M., and Jöckel, P.: A very limited role of tropospheric chlorine as a sink of the greenhouse gas methane,  
*Atmospheric Chemistry and Physics*, 18, 9831–9843, <https://doi.org/https://doi.org/10.5194/acp-18-9831-2018>, 2018.



- 455 Gupta, M., Tyler, S., and Cicerone, R.: Modeling atmospheric  $\delta^{13}\text{C}$  and the causes of recent changes in atmospheric  $\text{CH}_4$  amounts, *Journal of Geophysical Research: Atmospheres*, 101, 22 923–22 932, <https://doi.org/10.1029/96JD02386>, 1996.
- Hauglustaine, D. A., Hourdin, F., Jourdain, L., Filiberti, M.-A., Walters, S., Lamarque, J.-F., and Holland, E. A.: Interactive chemistry in the Laboratoire de Météorologie Dynamique general circulation model: Description and background tropospheric chemistry evaluation, *Journal of Geophysical Research: Atmospheres*, 109, <https://doi.org/10.1029/2003JD003957>, 2004.
- 460 Hauglustaine, D. A., Cozic, A., Caubel, A., Lathièrre, J., Sépulchre, P., Cohen, Y., Balkanski, Y., Lurton, T., Boucher, O., and Tsigaridis, K.: Coupled Climate-Chemistry-Aerosol simulations under the AerChemMIP scenarios with the IPSL-CM5A2-INCA climate model, in preparation, 2021.
- Hossaini, R., Chipperfield, M. P., Saiz-Lopez, A., Fernandez, R., Monks, S., Feng, W., Brauer, P., and von Glasow, R.: A global model of tropospheric chlorine chemistry: Organic versus inorganic sources and impact on methane oxidation, *Journal of Geophysical Research: Atmospheres*, 121, 14,271–14,297, <https://doi.org/10.1002/2016JD025756>, 2016.
- 465 Hourdin, F., Musat, I., Bony, S., Braconnot, P., Codron, F., Dufresne, J.-L., Fairhead, L., Filiberti, M.-A., Friedlingstein, P., Grandpeix, J.-Y., Krinner, G., LeVan, P., Li, Z.-X., and Lott, F.: The LMDZ4 general circulation model: climate performance and sensitivity to parametrized physics with emphasis on tropical convection, *Climate Dynamics*, 27, 787–813, <https://doi.org/10.1007/s00382-006-0158-0>, 2006.
- Houweling, S., Bergamaschi, P., Chevallier, F., Heimann, M., Kaminski, T., Krol, M., Michalak, A. M., and Patra, P.: Global inverse modeling of  $\text{CH}_4$  sources and sinks: an overview of methods, *Atmospheric Chemistry and Physics*, 17, 235–256, <https://doi.org/https://doi.org/10.5194/acp-17-235-2017>, 2017.
- 470 Karion, A., Sweeney, C., Tans, P., and Newberger, T.: AirCore: An Innovative Atmospheric Sampling System, *Journal of Atmospheric and Oceanic Technology*, 27, 1839–1853, <https://doi.org/10.1175/2010JTECHA1448.1>, 2010.
- Lassey, K. R., Lowe, D. C., and Manning, M. R.: The trend in atmospheric methane  $\delta^{13}\text{C}$  and implications for isotopic constraints on the global methane budget, *Global Biogeochemical Cycles*, 14, 41–49, <https://doi.org/10.1029/1999GB900094>, 2000.
- 475 Locatelli, R., Bousquet, P., Hourdin, F., Saunois, M., Cozic, A., Couvreux, F., Grandpeix, J.-Y., Lefebvre, M.-P., Rio, C., Bergamaschi, P., Chambers, S. D., Karstens, U., Kazan, V., van der Laan, S., Meijer, H. A. J., Moncrieff, J., Ramonet, M., Scheeren, H. A., Schlosser, C., Schmidt, M., Vermeulen, A., and Williams, A. G.: Atmospheric transport and chemistry of trace gases in LMDz5B: evaluation and implications for inverse modelling, *Geoscientific Model Development*, 8, 129–150, <https://doi.org/10.5194/gmd-8-129-2015>, 2015.
- 480 Louis, J.-F.: A parametric model of vertical eddy fluxes in the atmosphere, *Boundary-Layer Meteorology*, 17, 187–202, <https://doi.org/10.1007/BF00117978>, 1979.
- Mailler, S., Menut, L., Khvorostyanov, D., Valari, M., Couvidat, F., Siour, G., Turquety, S., Briant, R., Tuccella, P., Bessagnet, B., Colette, A., Létinois, L., Markakis, K., and Meleux, F.: CHIMERE-2017: from urban to hemispheric chemistry-transport modeling, *Geoscientific Model Development*, 10, 2397–2423, <https://doi.org/10.5194/gmd-10-2397-2017>, 2017.
- 485 McCarthy, M. C., Connell, P., and Boering, K. A.: Isotopic fractionation of methane in the stratosphere and its effect on free tropospheric isotopic compositions, *Geophysical Research Letters*, 28, 3657–3660, <https://doi.org/10.1029/2001GL013159>, 2001.
- McCarthy, M. C., Boering, K. A., Rice, A. L., Tyler, S. C., Connell, P., and Atlas, E.: Carbon and hydrogen isotopic compositions of stratospheric methane: 2. Two-dimensional model results and implications for kinetic isotope effects, *Journal of Geophysical Research: Atmospheres*, 108, <https://doi.org/10.1029/2002JD003183>, 2003.
- 490 McNorton, J., Wilson, C., Gloor, M., Parker, R. J., Boesch, H., Feng, W., Hossaini, R., and Chipperfield, M. P.: Attribution of recent increases in atmospheric methane through 3-D inverse modelling, *Atmospheric Chemistry and Physics*, 18, 18 149–18 168, <https://doi.org/https://doi.org/10.5194/acp-18-18149-2018>, 2018.



- Meinshausen, M., Vogel, E., Nauels, A., Lorbacher, K., Meinshausen, N., Etheridge, D. M., Fraser, P. J., Montzka, S. A., Rayner, P. J., Trudinger, C. M., Krummel, P. B., Beyerle, U., Canadell, J. G., Daniel, J. S., Enting, I. G., Law, R. M., Lunder, C. R., O'Doherty, S., Prinn, R. G., Reimann, S., Rubino, M., Velders, G. J. M., Vollmer, M. K., Wang, R. H. J., and Weiss, R.: Historical greenhouse gas concentrations for climate modelling (CMIP6), *Geoscientific Model Development*, 10, 2057–2116, <https://doi.org/10.5194/gmd-10-2057-2017>, 2017.
- Membrive, O., Crevoisier, C., Sweeney, C., Danis, F., Hertzog, A., Engel, A., Bönisch, H., and Picon, L.: AirCore-HR: a high-resolution column sampling to enhance the vertical description of CH<sub>4</sub> and CO<sub>2</sub>, *Atmos. Meas. Tech.*, p. 20, 2017.
- Menut, L., Bessagnet, B., Khvorostyanov, D., Beekmann, M., Blond, N., Colette, A., Coll, I., Curci, G., Foret, G., Hodzic, A., Mailler, S., Meleux, F., Monge, J.-L., Pison, I., Siour, G., Turquety, S., Valari, M., Vautard, R., and Vivanco, M. G.: CHIMERE 2013: a model for regional atmospheric composition modelling, *Geoscientific Model Development*, 6, 981–1028, <https://doi.org/10.5194/gmd-6-981-2013>, 2013.
- Monteil, G., Houweling, S., Dlugokenky, E. J., Maenhout, G., Vaughn, B. H., White, J. W. C., and Rockmann, T.: Interpreting methane variations in the past two decades using measurements of CH<sub>4</sub> mixing ratio and isotopic composition, *Atmospheric Chemistry and Physics*, 11, 9141–9153, <https://doi.org/10.5194/acp-11-9141-2011>, 2011.
- Müller, R., Brenninkmeijer, C. A. M., and Crutzen, P. J.: A Large <sup>13</sup>C deficit in the lower Antarctic stratosphere due to “ozone hole” chemistry: Part II, Modeling, *Geophysical Research Letters*, 23, 2129–2132, <https://doi.org/10.1029/96GL01472>, 1996.
- Neef, L., Weele, M. v., and Velthoven, P. v.: Optimal estimation of the present-day global methane budget, *Global Biogeochemical Cycles*, 24, <https://doi.org/10.1029/2009GB003661>, 2010.
- Nisbet, E. G., Manning, M. R., Dlugokenky, E. J., Fisher, R. E., Lowry, D., Michel, S. E., Myhre, C. L., Platt, S. M., Allen, G., Bousquet, P., Brownlow, R., Cain, M., France, J. L., Hermansen, O., Hossaini, R., Jones, A. E., Levin, I., Manning, A. C., Myhre, G., Pyle, J. A., Vaughn, B. H., Warwick, N. J., and White, J. W. C.: Very Strong Atmospheric Methane Growth in the 4 Years 2014–2017: Implications for the Paris Agreement, *Global Biogeochemical Cycles*, 33, 318–342, <https://doi.org/10.1029/2018GB006009>, 2019.
- Ostler, A., Sussmann, R., Patra, P. K., Houweling, S., Bruine, M. D., Stiller, G. P., Haenel, F. J., Plieninger, J., Bousquet, P., Yin, Y., Saunio, M., Walker, K. A., Deutscher, N. M., Griffith, D. W. T., Blumenstock, T., Hase, F., Warneke, T., Wang, Z., Kivi, R., and Robinson, J.: Evaluation of column-averaged methane in models and TCCON with a focus on the stratosphere, *Atmospheric Measurement Techniques*, 9, 4843–4859, <https://doi.org/10.5194/amt-9-4843-2016>, 2016.
- Parker, R. J., Webb, A., Boesch, H., Somkuti, P., Barrio Guillo, R., Di Noia, A., Kalaitzi, N., Anand, J. S., Bergamaschi, P., Chevallier, F., Palmer, P. I., Feng, L., Deutscher, N. M., Feist, D. G., Griffith, D. W. T., Hase, F., Kivi, R., Morino, I., Notholt, J., Oh, Y.-S., Ohyama, H., Petri, C., Pollard, D. F., Roehl, C., Sha, M. K., Shiomi, K., Strong, K., Sussmann, R., Té, Y., Velazco, V. A., Warneke, T., Wennberg, P. O., and Wunch, D.: A decade of GOSAT Proxy satellite CH<sub>4</sub> observations, *Earth System Science Data*, 12, 3383–3412, <https://doi.org/10.5194/essd-12-3383-2020>, 2020.
- Patra, P. K., Houweling, S., Krol, M., Bousquet, P., Belikov, D., Bergmann, D., Bian, H., Cameron-Smith, P., Chipperfield, M. P., Corbin, K., Fortems-Cheiney, A., Fraser, A., Gloor, E., Hess, P., Ito, A., Kawa, S. R., Law, R. M., Loh, Z., Maksyutov, S., Meng, L., Palmer, P. I., Prinn, R. G., Rigby, M., Saito, R., and Wilson, C.: TransCom model simulations of CH<sub>4</sub> and related species: linking transport, surface flux and chemical loss with CH<sub>4</sub> variability in the troposphere and lower stratosphere, *Atmospheric Chemistry and Physics*, 11, 12 813–12 837, <https://doi.org/10.5194/acp-11-12813-2011>, 2011.
- Pison, I., Bousquet, P., Chevallier, F., Szopa, S., and Hauglustaine, D.: Multi-species inversion of CH<sub>4</sub>, CO and H<sub>2</sub> emissions from surface measurements, *Atmos. Chem. Phys.*, p. 17, 2009.



- Rice, A. L., Tyler, S. C., McCarthy, M. C., Boering, K. A., and Atlas, E.: Carbon and hydrogen isotopic compositions of stratospheric methane: 1. High-precision observations from the NASA ER-2 aircraft, *Journal of Geophysical Research: Atmospheres*, 108, <https://doi.org/10.1029/2002JD003042>, 2003.
- 535 Rice, A. L., Butenhoff, C. L., Teama, D. G., Röger, F. H., Khalil, M. A. K., and Rasmussen, R. A.: Atmospheric methane isotopic record favors fossil sources flat in 1980s and 1990s with recent increase, *Proceedings of the National Academy of Sciences*, 113, 10 791–10 796, <https://doi.org/10.1073/pnas.1522923113>, 2016.
- Rigby, M., Manning, A. J., and Prinn, R. G.: The value of high-frequency, high-precision methane isotopologue measurements for source and sink estimation, *Journal of Geophysical Research: Atmospheres*, 117, <https://doi.org/10.1029/2011JD017384>, 2012.
- 540 Röckmann, T., Groöß, J.-U., and Müller, R.: The impact of anthropogenic chlorine emissions, stratospheric ozone change and chemical feedbacks on stratospheric water, *Atmospheric Chemistry and Physics*, 4, 693–699, <https://doi.org/10.5194/acp-4-693-2004>, 2004.
- Saueressig, G., Bergamaschi, P., Crowley, J. N., Fischer, H., and Harris, G. W.: Carbon kinetic isotope effect in the reaction of CH<sub>4</sub> with Cl atoms, *Geophysical Research Letters*, 22, 1225–1228, <https://doi.org/10.1029/95GL00881>, 1995.
- 545 Saueressig, G., Crowley, J. N., Bergamaschi, P., Brühl, C., Brenninkmeijer, C. A. M., and Fischer, H.: Carbon 13 and D kinetic isotope effects in the reactions of CH<sub>4</sub> with O(1 D) and OH: New laboratory measurements and their implications for the isotopic composition of stratospheric methane, *Journal of Geophysical Research: Atmospheres*, 106, 23 127–23 138, <https://doi.org/10.1029/2000JD000120>, 2001.
- Saunois, M., Stavert, A. R., Poulter, B., Bousquet, P., Canadell, J. G., Jackson, R. B., Raymond, P. A., Dlugokencky, E. J., Houweling, S., Patra, P. K., Ciais, P., Arora, V. K., Bastviken, D., Bergamaschi, P., Blake, D. R., Brailsford, G., Bruhwiler, L., Carlson, K. M., Carrol, M., Castaldi, S., Chandra, N., Crevoisier, C., Crill, P. M., Covey, K., Curry, C. L., Etiope, G., Frankenberg, C., Gedney, N., Hegglin, M. I., Höglund-Isaksson, L., Hugelius, G., Ishizawa, M., Ito, A., Janssens-Maenhout, G., Jensen, K. M., Joos, F., Kleinen, T., Krummel, P. B., Langenfelds, R. L., Laruelle, G. G., Liu, L., Machida, T., Maksyutov, S., McDonald, K. C., McNorton, J., Miller, P. A., Melton, J. R., Morino, I., Müller, J., Murguía-Flores, F., Naik, V., Niwa, Y., Noce, S., O'Doherty, S., Parker, R. J., Peng, C., Peng, S., Peters, G. P., Prigent, C., Prinn, R., Ramonet, M., Regnier, P., Riley, W. J., Rosentretter, J. A., Segers, A., Simpson, I. J., Shi, H., Smith, S. J., Steele, L. P., Thornton, B. F., Tian, H., Tohjima, Y., Tubiello, F. N., Tsuruta, A., Viovy, N., Voulgarakis, A., Weber, T. S., van Weele, M., van der Werf, G. R., Weiss, R. F., Worthy, D., Wunch, D., Yin, Y., Yoshida, Y., Zhang, W., Zhang, Z., Zhao, Y., Zheng, B., Zhu, Q., Zhu, Q., and Zhuang, Q.: The Global Methane Budget 2000–2017, *Earth System Science Data*, 12, 1561–1623, <https://doi.org/https://doi.org/10.5194/essd-12-1561-2020>, 2020.
- 555 Schaefer, H., Fletcher, S. E. M., Veidt, C., Lassey, K. R., Brailsford, G. W., Bromley, T. M., Dlugokencky, E. J., Michel, S. E., Miller, J. B., Levin, I., Lowe, D. C., Martin, R. J., Vaughn, B. H., and White, J. W. C.: A 21st-century shift from fossil-fuel to biogenic methane emissions indicated by <sup>13</sup>CH<sub>4</sub>, *Science*, 352, 80–84, <https://doi.org/10.1126/science.aad2705>, 2016.
- Schwietzke, S., Sherwood, O. A., Bruhwiler, L. M. P., Miller, J. B., Etiope, G., Dlugokencky, E. J., Michel, S. E., Arling, V. A., Vaughn, B. H., White, J. W. C., and Tans, P. P.: Upward revision of global fossil fuel methane emissions based on isotope database, *Nature*, 538, 88–91, <https://doi.org/10.1038/nature19797>, 2016.
- 565 Sherwen, T., Schmidt, J. A., Evans, M. J., Carpenter, L. J., Großmann, K., Eastham, S. D., Jacob, D. J., Dix, B., Koenig, T. K., Sinreich, R., Ortega, I., Volkamer, R., Saiz-Lopez, A., Prados-Roman, C., Mahajan, A. S., and Ordóñez, C.: Global impacts of tropospheric halogens (Cl, Br, I) on oxidants and composition in GEOS-Chem, *Atmospheric Chemistry and Physics*, 16, 12 239–12 271, <https://doi.org/https://doi.org/10.5194/acp-16-12239-2016>, 2016.



- Sherwood, O. A., Schwietzke, S., Arling, V. A., and Etiope, G.: Global Inventory of Gas Geochemistry Data from Fossil Fuel, Microbial and Burning Sources, version 2017, Earth System Science Data, 9, 639–656, <https://doi.org/10.5194/essd-9-639-2017>, 2017.
- 570 Stolper, D. A., Sessions, A. L., Ferreira, A. A., Santos Neto, E. V., Schimmelmann, A., Shusta, S. S., Valentine, D. L., and Eiler, J. M.: Combined  $^{13}\text{C}$ –D and D–D clumping in methane: Methods and preliminary results, *Geochimica et Cosmochimica Acta*, 126, 169–191, <https://doi.org/10.1016/j.gca.2013.10.045>, 2014.
- Strode, S. A., Wang, J. S., Manyin, M., Duncan, B., Hossaini, R., Keller, C. A., Michel, S. E., and White, J. W. C.: Strong sensitivity of the isotopic composition of methane to the plausible range of tropospheric chlorine, *Atmospheric Chemistry and Physics*, 20, 8405–8419, <https://doi.org/10.5194/acp-20-8405-2020>, 2020.
- 575 Takigawa, M., Takahashi, M., and Akiyoshi, H.: Simulation of ozone and other chemical species using a Center for Climate System Research/National Institute for Environmental Studies atmospheric GCM with coupled stratospheric chemistry, *Journal of Geophysical Research: Atmospheres*, 104, 14 003–14 018, <https://doi.org/10.1029/1998JD100105>, 1999.
- Terrenoire, E., Hauglustaine, D., Gasser, T., and Penanhoat, O.: The impact of carbon dioxide aviation emissions on future climate change, in: 1st Edition of the Aerospace Europe Conference – AEC2020, Bordeaux, France, <https://hal.archives-ouvertes.fr/hal-02859983>, 2020.
- Thanwerdas, J., Saunois, M., Berchet, A., Pison, I., Vaughn, B. H., Michel, S. E., and Bousquet, P.: Variational inverse modelling within the Community Inversion Framework to assimilate  $\delta^{13}\text{C}(\text{CH}_4)$  and  $\text{CH}_4$ : a case study with model LMDz-SACS, *Geoscientific Model Development Discussions*, pp. 1–29, <https://doi.org/10.5194/gmd-2021-106>, 2021.
- Thompson, R. L., Nisbet, E. G., Pissot, I., Stohl, A., Blake, D., Dlugokencky, E. J., Helmig, D., and White, J. W. C.: Variability in Atmospheric Methane From Fossil Fuel and Microbial Sources Over the Last Three Decades, *Geophysical Research Letters*, 45, 11,499–11,508, <https://doi.org/10.1029/2018GL078127>, 2018.
- 585 Tiedtke, M.: A Comprehensive Mass Flux Scheme for Cumulus Parameterization in Large-Scale Models, *Monthly Weather Review*, 117, 1779–1800, [https://doi.org/10.1175/1520-0493\(1989\)117<1779:ACMFSF>2.0.CO;2](https://doi.org/10.1175/1520-0493(1989)117<1779:ACMFSF>2.0.CO;2), 1989.
- Wang, J. S., McElroy, M. B., Spivakovsky, C. M., and Jones, D. B. A.: On the contribution of anthropogenic Cl to the increase in  $\delta^{13}\text{C}$  of atmospheric methane: ANTHROPOGENIC Cl AND  $\delta^{13}\text{C}$  OF METHANE, *Global Biogeochemical Cycles*, 16, 20–1–20–11, <https://doi.org/10.1029/2001GB001572>, 2002.
- 590 Wang, X., Jacob, D. J., Eastham, S. D., Sulprizio, M. P., Zhu, L., Chen, Q., Alexander, B., Sherwen, T., Evans, M. J., Lee, B. H., Haskins, J. D., Lopez-Hilfiker, F. D., Thornton, J. A., Huey, G. L., and Liao, H.: The role of chlorine in global tropospheric chemistry, *Atmospheric Chemistry and Physics*, 19, 3981–4003, <https://doi.org/10.5194/acp-19-3981-2019>, 2019.
- 595 Wang, X., Jacob, D. J., Downs, W., Zhai, S., Zhu, L., Shah, V., Holmes, C. D., Sherwen, T., Alexander, B., Evans, M. J., Eastham, S. D., Neuman, J. A., Veres, P., Koenig, T. K., Volkamer, R., Huey, L. G., Bannan, T. J., Percival, C. J., Lee, B. H., and Thornton, J. A.: Global tropospheric halogen (Cl, Br, I) chemistry and its impact on oxidants, *Atmospheric Chemistry and Physics Discussions*, pp. 1–34, <https://doi.org/10.5194/acp-2021-441>, 2021.
- Warwick, N. J., Cain, M. L., Fisher, R., France, J. L., Lowry, D., Michel, S. E., Nisbet, E. G., Vaughn, B. H., White, J. W. C., and Pyle, J. A.: Using  $\delta^{13}\text{C}$ – $\text{CH}_4$  and  $\delta\text{D}$ – $\text{CH}_4$  to constrain Arctic methane emissions, *Atmospheric Chemistry and Physics*, 16, 14 891–14 908, <https://doi.org/10.5194/acp-16-14891-2016>, 2016.
- 600 White, J. W. C., Vaughn, B. H., and Michel, S. E.: Stable isotopic composition of atmospheric methane ( $^{13}\text{C}$ ) from the NOAA ESRL Carbon Cycle Cooperative Global Air Sampling Network, 1998–2018, available at [ftp://aftp.cmdl.noaa.gov/data/trace\\_gases/ch4c13/flask/](ftp://aftp.cmdl.noaa.gov/data/trace_gases/ch4c13/flask/), last access: 12 July 2021, 2021.